Spirit rover localization and topographic mapping at the landing site of Gusev crater, Mars

Rongxing Li,[1] Brent A. Archinal,[2] Raymond E. Arvidson,[3] Jim Bell,[4] Philip Christensen,[5] Larry Crumpler,[6] David J. Des Marais,[7] Kaichang Di,[1] Tom Duxbury,[8] Matt Golombek,[8] John Grant,[9] Ronald Greeley,[5] Joe Guinn,[8] Andrew Johnson,[8] Randolph L. Kirk,[2] Mark Maimone,[8] Larry H. Matthies,[8] Mike Malin,[10] Tim Parker,[8] Mike Sims,[7] Shane Thompson,[5] Steven W. Squyres,[4] and Larry A. Soderblom[2]

Received 2 May 2005; revised 8 June 2005; accepted 24 June 2005; published 12 January 2006.

[1] By sol 440, the Spirit rover has traversed a distance of 3.76 km (actual distance traveled instead of odometry). Localization of the lander and the rover along the traverse has been successfully performed at the Gusev crater landing site. We localized the lander in the Gusev crater using two-way Doppler radio positioning and cartographic triangulations through landmarks visible in both orbital and ground images. Additional high-resolution orbital images were used to verify the determined lander position. Visual odometry and bundle adjustment technologies were applied to compensate for wheel slippage, azimuthal angle drift, and other navigation errors (which were as large as 10.5% in the Husband Hill area). We generated topographic products, including 72 ortho maps and three-dimensional (3-D) digital terrain models, 11 horizontal and vertical traverse profiles, and one 3-D crater model (up to sol 440). Also discussed in this paper are uses of the data for science operations planning, geological traverse surveys, surveys of wind-related features, and other science applications.

Citation: Li, R., et al. (2006), Spirit rover localization and topographic mapping at the landing site of Gusev crater, Mars, *J. Geophys. Res.*, *111*, E02S06, doi:10.1029/2005JE002483.

1. Introduction

[2] Localization of the Spirit rover has been important for understanding where the vehicle has traversed and for planning traverses to new locations [*Arvidson et al.*, 2004], particularly ones identified in orbital images. The rover's mission has taken it over a long traverse (over 3.76 km by sol 440) from the Columbia Memorial Station (the lander), toward Bonneville crater, across the Gusev plains for a distance of 2.7 km, and onto the flanks of Husband Hill (one of the hills in the Columbia Hills complex). Remote sensing observations using Pancam [*Bell et al.*, 2006] and Mini-TES (P. R. Christensen et al., Mini-TES overview, manuscript in preparation, 2005), along with orbital images were used to identify targets for detailed study. The rover was then commanded to traverse to these targets, with fine-scale positioning used to place the vehicle in locations where the instrument deployment device (IDD) could be used to place other instruments onto surfaces for acquisition of in situ observations. All of these operations demanded accurate three-dimensional (3-D) location information. Furthermore, localization for traverses and conversion to the Mars inertial coordinate system and MBF (Mars body-fixed) coordinate system [*Li et al.*, 2004] were necessary to be able to place rover-based observations into the regional-scale context seen from orbital images.

[3] This paper focuses on results of lander and rover localization and topographic mapping of the MER 2003 mission at Gusev crater, through sol 440 of the Spirit rover. We localized the lander in Gusev crater using two-way Doppler radio positioning and cartographic triangulations through landmarks visible in both orbital and ground images. Additional high-resolution orbital images were used to verify the determined lander position. Visual odometry (VO) (on board) and bundle adjustment (BA) (on Earth) technologies were applied to correct errors caused by wheel slippage and azimuthal angle drift. BA builds a ground image network and estimates precision rover positions and image orientation through an optimization process. It enabled correction of an accumulated 56.59 m rover position

[1]Department of Civil and Environmental Engineering and Geodetic Science, Ohio State University, Columbus, Ohio, USA.
[2]U.S. Geological Survey, Flagstaff, Arizona, USA.
[3]Department of Earth and Planetary Sciences, Washington University, St. Louis, Missouri, USA.
[4]Department of Astronomy, Cornell University, Ithaca, New York, USA.
[5]Department of Geological Sciences, Arizona State University, Tempe, Arizona, USA.
[6]New Mexico Museum of Natural History and Science, Albuquerque, New Mexico, USA.
[7]NASA Ames Research Center, Moffett Field, California, USA.
[8]Jet Propulsion Laboratory, Pasadena, California, USA.
[9]Smithsonian Institution, Washington, DC, USA.
[10]Malin Space Science Systems, San Diego, California, USA.

0148-0227/06/2005JE002483$09.00

error over a distance of 540.88 m (10.5%) during the ascent of Husband Hill. Over the course of the Spirit mission, we generated topographic products including 72 ortho maps and 3-D digital terrain models (DTMs), 11 horizontal rover traverse maps, vertical traverse profiles up to sol 440, and one 3-D crater model.

2. Global and Local Reference Systems

[4] The Mars global reference systems include the Mars inertial reference system and the Mars body-fixed reference system [*Li et al.*, 2004]. The inertial reference system is the International Celestial Reference Frame [*Ma et al.*, 1998], with an origin at the center of mass of Mars. It is mainly used for navigation of orbital spacecraft and for localization of the lander and tracking of the rover through radio tracking from the Earth or Mars orbit. Like the inertial reference system, the Mars body-fixed reference system uses the center of mass of Mars as its origin and a specified orientation that matches Mars rotation and pole position [*Seidelmann et al.*, 2002]. The shape of the Martian surface in the body-fixed reference system used in the MER mission is approximated by a sphere where north latitude and east longitude are positive. To specify the elevation, a planetary radius (in kilometers or meters) is given along with its latitude and longitude. The Mars body-fixed reference system can be used for mapping ground features observed from orbiting spacecraft.

[5] Once Spirit landed on the Martian surface, a Landing Site Cartographic (LSC) reference system was established. The LSC is an east-north-up (X-Y-Z) right-handed local system with its origin at the lander within the landing site, which is designated the Columbia Memorial Station. The orientation of the axes was determined using the rover's inertial measurement unit (IMU) and Sun-finding techniques using Pancam images. Rover locations and landing site cartographic products are calculated and generated in the LSC reference system.

[6] Several local reference systems are also used. For example, the Surface Fixed Reference System (S frame) has its origin fixed to the lander, just like the LSC. It is a northeast-down (X-Y-Z) right-handed reference system. A site reference system (site frame) is defined locally within an area to locate the rover and ground features. A new site frame is defined usually as the rover moves a significant distance, for instance, over 50 m. The nth site frame is generated by using the last rover trajectory in the (n − 1)th site frame. The initial site frame is the same as the S frame. Transformations between site frames and the LSC frame are calculated through the translations and orientations between the site frames and the S frame. Although ground data are collected in the site frames, derived rover locations and topographic mapping products are all presented in the LSC frame for consistent referencing and regional context.

[7] Rover images, including Pancam, Navcam (J. N. Maki et al., An overview of Spirit Navcam and Hazcam observations on Mars: Sols 1 through 400, manuscript in preparation, 2005; hereinafter referred to as Maki et al., manuscript in preparation, 2005) and Hazcam (Maki et al., manuscript in preparation, 2005) images, are first referenced to the rover frame through its camera model (CAHVOR model), and is then further referenced to a site frame. The rover frame has its origin on the rover and is a forward-right-down (X-Y-Z) right-handed reference system. The CAHVOR model is a camera model used in computer vision field and has a wide usage in planetary robotic applications [*Yakimovsky and Cunningham*, 1978; *Gennery*, 1992]. A conversion is carried out from the CAHVOR model to a photogrammetric model [*Di and Li*, 2004] that uses LSC and is appropriate for the incremental bundle adjustment technology for creating accurate rover locations and mapping products.

3. Prelanding Mapping

[8] Before landing, potential landing sites were mapped by using orbital images from Viking, Mars Orbital Camera (MOC), and thermal emission imaging system (THEMIS) imaging systems. Some limited areas were covered by stereo MOC images formed by overlapping in the cross-track direction.

[9] Mars Digital Image Mosaics (MDIMs) are a standard product made available by the U.S. Geological Survey (USGS) in versions MDIM 1, color MDIM, and MDIM 2.0 [*U.S. Geological Survey*, 1991; *Batson and Eliason*, 1995; *Kirk et al.*, 1999, 2000]. The MDIMs use Viking images and have 256 pixels/degree (approximately 231 m/pixel at the equator). They are projected using an equirectangular projection. The most recent version of MDIM is 2.1; mosaics are referenced by MOLA tie points.

[10] Mosaics using MOC wide-angle (WA) and narrow-angle (NA) images were available from Malin Space Science Systems with a resolution of 256 pixel/degree and 3–5 m/pixel, respectively [*Caplinger*, 2005] (see also http://www.msss.com/mgcwg/mgm). The mosaics are often "uncontrolled" in that the imaging geometry is computed solely from the pointing information of the orbital telemetry without any further adjustment. Similar mosaics of THEMIS VIS (Visual Imager) images (resolution 19 m/pixel) were produced by the Arizona State University (P. R. Christensen, personal communication, 2004) (see also http://www.mars.asu.edu/~gorelick/mos/mex_merge/index.html). Specific mosaics of MOC NA (resolution 3–5 m) for the two MER landing sites were produced by JPL and members of the Mars Geodesy and Cartography Working Group (MGCWG). These mosaics have a grid interval of 0.5° and a subgrid interval of 0.1°. Each mosaic was overlaid with a landing ellipse whose size had been decreased to 78 km (major axis) by 10 km (minor axis) from larger ellipses as knowledge of the spacecraft orbit and navigation improved greatly before landing (Figure 1).

[11] The MOLA topographic models are available at both landing sites. Despite their high vertical accuracy, their primary limitations are imposed by the along-track (about 300 m) and between-track (about 1–2 km) footprint spacing, with gaps of up to 12 km at the equator [*Neumann et al.*, 2001]. Within the originally planned rover traversing areas of the landing site, there are a very limited number of MOLA grid points. An effort was made at the Mapping and Geographic Information System (GIS) Laboratory of The Ohio State University to register MOC NA imagery with the MOLA data. Using the rover parameters and Pancam and Navcam camera models, a set of ground features, such as craters and mountain peaks which could be expected to be

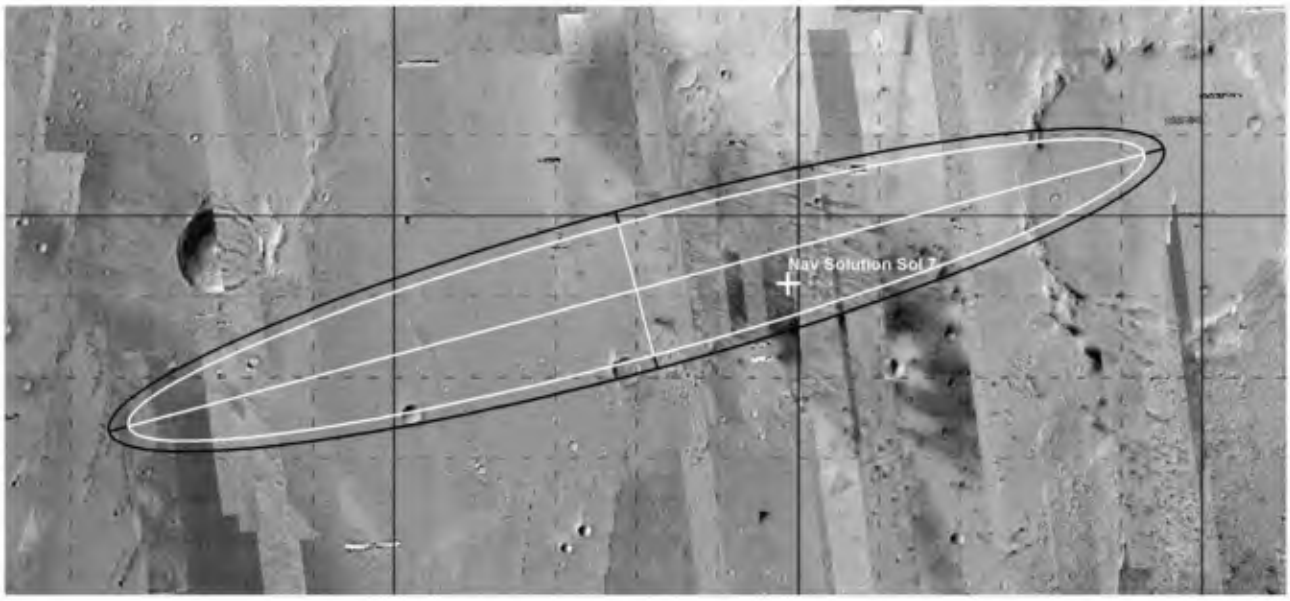

Figure 1. Orbital mosaic and landing ellipse. The background is the thermal emission imaging system (THEMIS) daytime thermal images (100 m/pixel) and Mars orbiting camera (MOC) NA images (thin image strips). The size of the landing ellipse was reduced from larger ellipses (e.g., the black one), and the white ellipse is the final one. The actual landing position is marked by the cross.

seen by the rover once it landed, were selected. The result helped the selection of ground features seen from the rover that can be linked to orbital images.

4. Localization of the Lander

[12] On 4 January 2004, the Spirit rover landed in Gusev crater. Determining where the lander is located within the landing ellipse in the Mars global reference system (either the inertial reference system or MBF) and with respect to other surface features in the LSC as soon as possible after landing was critical for planning science and engineering activities in the initial stages of rover exploration and for identifying other nearby features to plan the long-range rover traverse over the course of the mission. This was accomplished within eight days of landing (before the rover drove off the lander). This activity involved Doppler positioning in the inertial reference frame; reconstructing the entry, descent and landing (EDL) process using returned descent image motion estimation system (DIMES) images (A. Johnson, unpublished manuscript, 2004); and locating common features in the lander, descent, and orbiter images.

[13] The navigation team determined the location of the lander by fitting direct-to-Earth (DTE) two-way X-band Doppler signals from sol 2 to sol 4 and two passes of UHF two-way Doppler signals between Spirit and the Mars Odyssey orbiter. The Spirit lander location was determined in the inertial reference system and transformed to the MBF system (MOLA IAU 2000) as (14.571892°S, 175.47848°E), 12 km east of the landing ellipse center (Figures 1 and 2) [*Guinn and Ely*, 2004; *Golombek and Parker*, 2004]. After sol 1, when the first Navcam panorama was acquired, and later after the first Pancam panorama (Figure 3) was acquired (note that the first Pancam pan was not acquired on sol 1), various efforts were made to correlate ground features such as hills and craters in both the lander

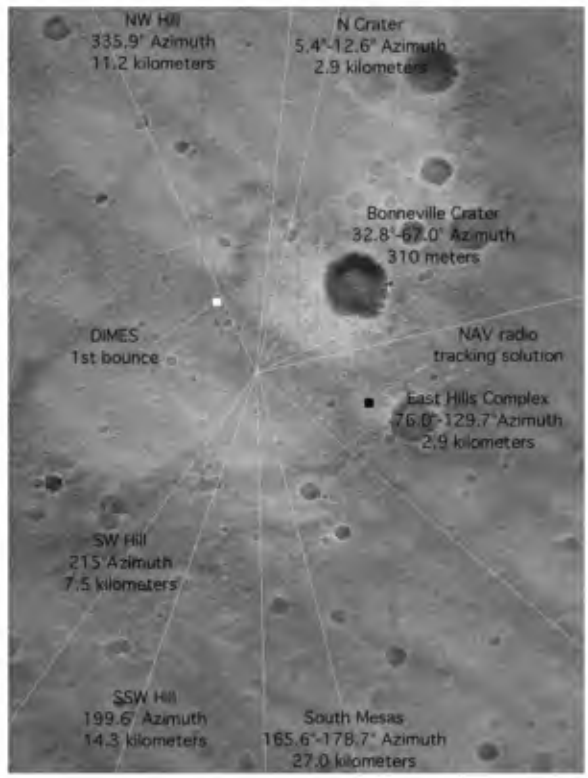

Figure 2. Spirit lander localization: high-resolution descent image motion estimation system (DIMES) and MOC mosaic of area around the Spirit lander. The black square shows the location of the navigation solution described in the text. The white square shows the first bounce point from the DIMES entry, descent and landing (EDL) reconstruction. Lines show azimuths to crater rims and hills clearly visible from the Spirit lander.

Figure 3. First Pancam panorama (360°) taken at the lander where the corresponding crater rims and hills in the mosaic of Figure 2 can be seen.

panoramas with features observed in the DIMES descent and MOC images. Among them are the most distinguishable features of the East Hill complex and Southwest Hill that were later unofficially named the Columbia Hills complex (about 2.7 km from the lander) and Grissom Hill (about 7.5 km from the lander) respectively, along with other hills and craters. These directional measurements were made either at a distinguished point (e.g., a hill peak) or on the boundary of a feature (e.g., both sides of a crater rim). The optimal cartographic triangulation resulted in the lander location (14.5692°S, 175.4729°E) (Figure 2) [*Golombek and Parker*, 2004; *Parker et al.*, 2004]. This lander location was later named the Columbia Memorial Station.

[14] Figure 4 shows (a) the location of the Spirit lander determined by the above cartographic triangulation and its corresponding location to the southeast (marked inertial) estimated by fitting direct-to-Earth two-way X-band Doppler radio transmissions and two passes of UHF two-way Doppler between Spirit and Mars Odyssey at the landing site, and (b) the rover location on sol 98 computed by rover sensors and ground images as well as its corresponding location to the southeast (marked inertial) determined by two passes of UHF two-way Doppler between Spirit and Mars Odyssey at the rover location on sols 94–98 where the rover paused for a flight software upload. During the period of the software upload, the Spirit rover was south of Bonneville crater at (14.5673°S, 175.4779°E) in MBF (MOLA IAU 2000 cartographic reference frame). In inertial space translated to the MOLA IAU 2000 frame the Spirit rover at the software upload was located at (14.570105°S, 175.48345°E). At landing, the inertial location was displaced to the southeast by 370 m at an azimuth of 116°. At software upload, the inertial location is displaced to the southeast by 360 m at an azimuth of 117°. The fact that the offset is so similar in azimuth and distance at both locations suggests that both the inertial and cartographic localization techniques are robust and accurate and no unaccounted for random errors exist in either. The observed systematic offset is most likely an offset between the cartographic frame and the inertial frame, and the observed offset is close to the 3 sigma estimate in prelanding maps [*Golombek and Parker*, 2004].

[15] The navigation solutions are useful, for example, for applications related to the Mars Odyssey or MGS orbiters and the Deep Space Network (DSN). On the other hand, cartographic solutions are required for most practical applications that refer to a map or the location of the rover with respect to other surface features. The MOC NA imager was targeted at the estimated lander location and acquired a new, high-resolution (1 m) compensated pitch and roll targeted observations (cPROTO) image at the Gusev site on sol 16, which is georeferenced and integrated in to a MOC NA mosaic in Figure 5a. Using the MOC NA images acquired before landing and the MOC cPROTO images acquired after landing, the location of the lander was verified through direct detection in images.

5. Rover Localization

[16] The rover has several driving modes, including blind driving and autonomous driving. In the autonomous drive mode, hazard avoidance is performed in real time using Hazcam stereo images and onboard navigation software. There is no hazard avoidance processing in the blind drive mode. In a typical driving sol, the rover first performs a blind drive for a distance that can be visualized and accurately measured from Pancam or Navcam images, and then performs an autonomous drive until a time that is typically set by energy constraints. Because autonomous driving is computation-intensive and hence slow, the autonomous portion of a drive often covers less distance than the blind portion.

[17] The Spirit rover egressed the lander on sol 12 and started a journey of 3.76 km (by sol 440, as plotted in Figure 5a) from the Columbia Memorial Station to Bonneville crater, and then to Columbia Hills. The uphill drive toward Bonneville crater typically covered 20–30 m on a driving sol with some slippage when approaching the rim of the crater. The long traverse of 2.7 km from Bonneville to Columbia Hills was achieved within 72 sols by a disciplined

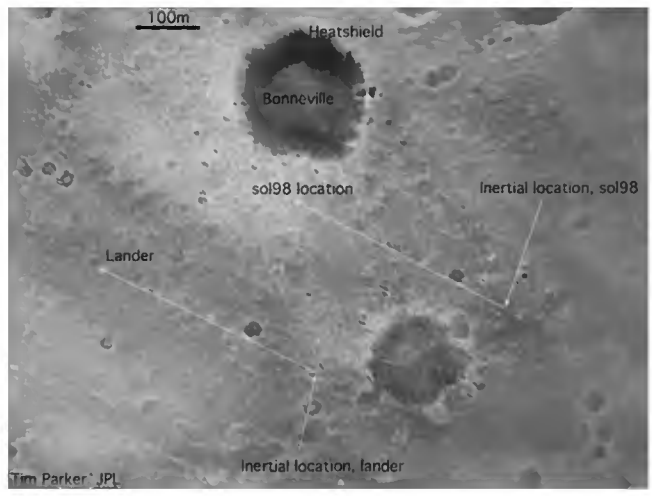

Figure 4. Spirit rover locations determined by cartographic triangulation and radio science based on navigation techniques at the lander position (marked "Lander" and "Inertial location, lander," respectively) and the software upload location (marked "sol98 location" and "Inertial location, sol98," respectively) as well as their offset vectors at the Gusev crater site.

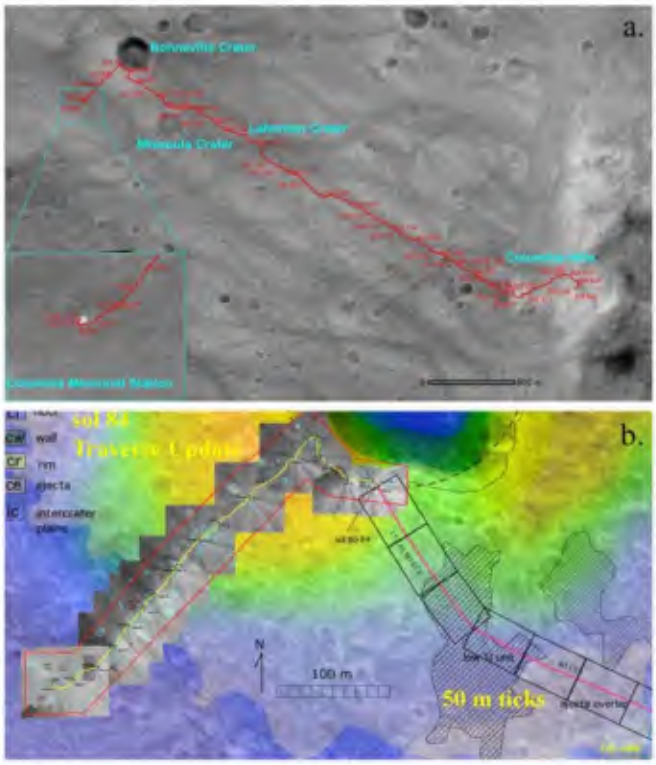

Figure 5. (a) Traverse of MER A, with a mosaic of two MOC compensated pitch and roll targeted observations (cPROTO) images and a regular MOC NA image as background. Bright pixels in the inset represent the lander/rover. (b) Traverse planning map for approaching Columbia Hills. The yellow line is the rover traverse along which are ortho maps and hollows marked in light blue. The red line after sol 84 is the planned traverse, segmented into 50 m ticks for planning purposes.

approach that combined a strategic goal (reaching the base of the hills by no later than sol 160) with tactical implementation (well-planned drives of up to 100 m per sol) as illustrated in Figure 5b. A drive metrics table was set for

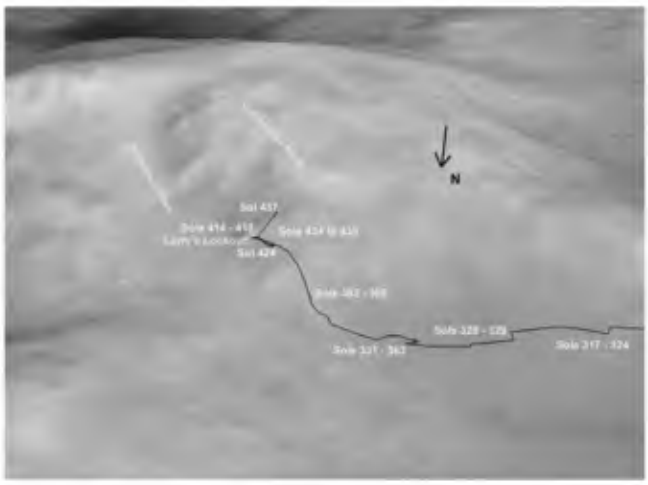

Figure 6. Rover traverse (black) projected onto the digital terrain model (DTM) of Husband Hill.

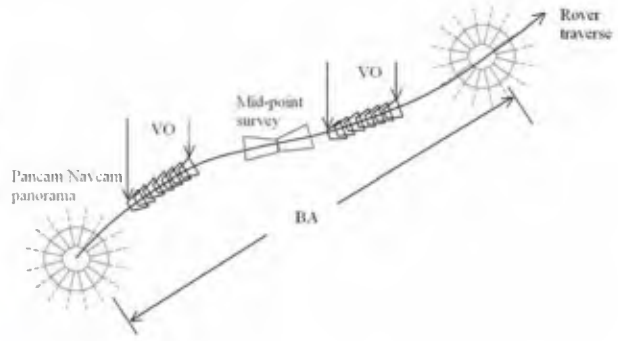

Figure 7. Configuration of images collected for localization and mapping: panoramas, visual odometry (VO) images, and middle point survey.

climbing Husband Hill where the horizontal distance and elevation increment were measured each sol against a reference elevation point (Figure 6).

[18] Rover localization has been conducted at several levels [*Li et al.*, 2004]. Within each sol cycle, the onboard IMU-based and wheel odometry-based localizations were regularly performed, supported irregularly (e.g., every ~10 sols) by Sun-finding techniques to improve the attitude knowledge. Rover position information has been generally of good quality and contained positional errors within 10%. The information was incorporated into the header of image files and a rover master file used to update the site frames, usually a few hours after downlink. In some cases where rover planners anticipated slippage caused by traversing on loose soil terrain or against steep slopes the onboard visual odometry (VO) became a necessary tool. VO was also used whenever accurate rover positions were desirable. In general, VO acquires consecutive Navcam stereo pairs within a traverse segment between two rover locations whereas Navcam or Pancam panoramas were often taken on separate sols (Figure 7). For localization purposes, survey images were often acquired near the midpoint of long drives. These usually were Navcam images taken either straight forward and backward or at 45° forward and backward on each side. Finally, the bundle adjustment technique combines the results of IMU/wheel odometry, VO, and localization images and builds an image network along the traverse to achieve a high-accuracy solution of rover positions of the entire traverse. BA was conducted on the ground (Earth).

5.1. Visual Odometry

[19] The MER rovers update their onboard estimate of rover position and orientation at 8 Hz. Changes in attitude (roll, pitch, yaw) are measured using a Litton LN-200 IMU that has three-axis accelerometers and three-axis angular rate sensors; changes in position are estimated based on the IMU data and how much the wheels have turned (wheel odometry). Both blind and autonomous drive motions are typically based on simple primitive operations: straight line drives, curved arcs, or turns in place [*Biesiadecki and Maimone*, 2005].

[20] In between driving primitives, the rover can make use of camera-based visual odometry to correct the errors in the initial wheel odometry-based estimates that occur when

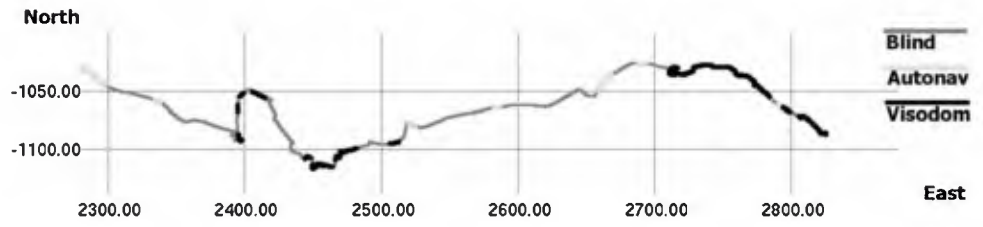

Figure 8. VO used extensively during the climbing of Husband Hill from sol 152 to sol 408: blind drive, autonav, and VO (Visodom) are represented by different line patterns. The horizontal axis is east, and the vertical axis is north.

the wheels lose traction, for example, on large rocks and steep slopes. The visual odometry system computes an update to the rover pose (x, y, z, roll, pitch, yaw) by tracking the motion of "interesting" terrain features between two consecutive pairs of stereo images in both 2-D pixel coordinates and 3-D ground coordinates.

[21] A set of potentially interesting features are found in the first left image using the Förstner interest operator, and a subset that spans the complete image is chosen. These are then projected into the second left image and matched using correlation. Several consistency checks are applied to filter out incorrect matches, including 3-D ray gap analysis, a rigidity check and an iterative random sample consensus (RANSAC) process. Finally, a maximum likelihood estimator is applied to the computed 3-D offsets to produce the final motion estimate. However, if any of the consistency checks fail, too few feature points are detected, or the estimation procedure fails to converge, then no motion estimate update will be produced and the initial estimate (based on wheel odometry) will be maintained. A more detailed description of this algorithm can be found by *Olson et al.* [2003] and *Li et al.* [2004].

[22] To ensure that enough features can be tracked, an overlap of at least 60% between adjacent images is recommended, and therefore all visual odometry drives are split into several small steps. During each step the rover is typically commanded to drive no more than 75 cm in a straight line or curved arc, and when turning in place is commanded to change heading by no more than 18° per step. Although visual odometry processing could be beneficial during all rover movements, each step requires over two minutes of processing time on MER's 20 MHz RAD6000 CPU. For this reason, visual odometry is only used in circumstances, such as high slip or a need for high-precision placement, that clearly require it. The onboard IMU has exhibited a very small drift rate (usually less than 3° per hour of operation) and therefore maintains attitude knowledge very well.

[23] As of March 2005, visual odometry on Spirit converged to a solution 590 out of 609 times in 52 sols. Instances where it failed to converge are primarily attributable to either too large a motion (e.g., commanding a 40° turn in place which resulted in too little image overlap) or lack of features in the imaged terrain. It successfully measured slips as high as 125% on sol 206 when Spirit tried to drive up a more than 25° slope. The longest drive with VO was 19.6 m on sol 381. Figure 8 shows all segments along the traverse from sol 152 to sol 408 during the climbing of Husband Hill where the traverse is represented by three different patterns to indicate blind, autonav, and VO (Visodom) drives.

5.2. Incremental Bundle Adjustment

[24] Positions computed based on telemetry data are generally within the nominal accuracy of 10%. The overall traverse accuracy by sol 440 was 1.5%, or a 56 m error over the entire 3.76 km traverse. This is a very impressive performance by the Spirit rover. However, larger errors occurred, for example during the climbing of Husband Hill, which accumulated to an accuracy of 10.5%. If large errors take place in a relatively small local area, the telemetry data would not be able to control images that are either taken at two different locations or in two rover sites (e.g., over 25 m apart). It would then be difficult to reference geological features across the area in a regional context. Furthermore, some traverse errors such as distance and azimuth drift errors may be accumulated across the landing site. As the rover traverses a long distance, the relative error may be small. However, local errors may be significant enough to affect mapping capability and the orbital images may have greater errors in a large area, so that rover positions and ground map features would not be matched.

[25] Images used in bundle adjustment are linearized (epipolar) images with practically no y parallax. The CAHV camera model, which is defined in the rover frame, is included in the image header. The position and attitude of each rover frame with respect to its site frame is defined by three translations and a set of quaternion parameters, which are also included in the image header. We first convert the CAHV camera model to a photogrammetric model that is necessary for BA and is commonly used in topographic mapping and remote sensing [*Di and Li*, 2004]. The camera model is then transformed in the site frame and subsequently in the LSC. Such information originates from telemetry data and is used as initial information in BA. Whenever VO is performed, its result is automatically supplied within the image header and also used in BA as initial information.

[26] As depicted in Figure 7, panoramas and traversing stereo images of Pancam and Navcam were taken at different locations. The Pancam panoramas were acquired mainly at locations where substantial science exploration activities took place, while Navcam panoramas were taken more frequently for navigation and near-rover site characterization. The purpose of BA of the image network is to optimally (in a least squares sense) adjust the pointing parameters (camera center position and three rotation angles) of each image in the network as well as to adjust the 3-D positions of the tie points. In this way, BA provides

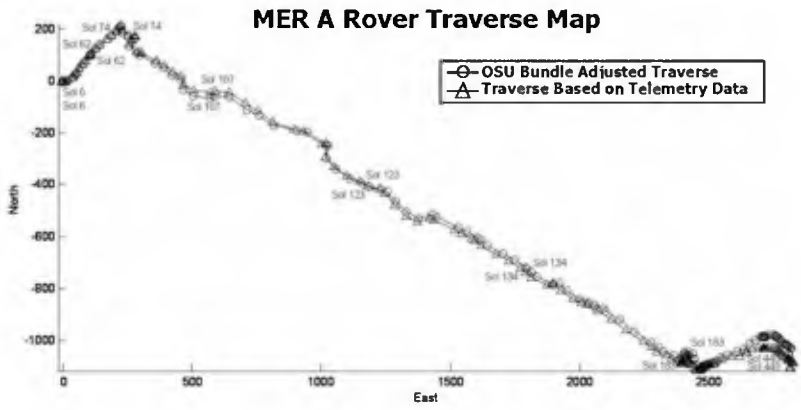

Figure 9. Spirit rover traverse up to sol 440. The line with triangular points is the traverse computed from telemetry data, and the line with circular points is the resulted/corrected traverse by the bundle adjustment method.

optimal rover positions at the times when the images were taken. A new incremental bundle adjustment method was developed [*Li et al.*, 2002, 2004] and employed to perform sol-by-sol BA operations.

[27] The success of bundle adjustment depends heavily on the tie points that are used to connect the rover images. In order to build a geometrically strong image network, a sufficient number of well-distributed tie points must be extracted and selected to link all the images processed. We developed a method that can automatically extract tie points from the intrastereo and interstereo panoramic Navcam and Pancam images [*Xu et al.*, 2002; *Di et al.*, 2002; *Li et al.*, 2003] (see http://astrogeology.usgs.gov/Projects/ISPRS/MEETINGS/Houston2003/abstracts/L1_isprs_mar03.pdf). In a typical Navcam and Pancam panorama, over 90% of the tie points can be selected automatically within each site. During the MER mission operations, this automation process greatly reduced the amount of tedious manual tie point selection work and speeded up the rover localization and map production process. However, selection of cross-site tie points (tie points between images taken in different site frames) remains a very challenging task and is currently done manually.

[28] Since there is no absolute control on the Martian surface, the accuracy of the BA is estimated using discrepancies computed from 2-D image coordinates and 3-D ground coordinates of bundle-adjusted cross-site and interstereo tie points that are projected from different stereo pairs. Specifically, the 3-D accuracy is derived from differences of 3-D ground coordinates of the cross-site tie points triangulated from different site frames. The 2-D accuracy is estimated by using differences between image coordinates of the same interstereo and cross-site tie points, which are measured in one stereo pair and projected from one or more stereo pairs (neighboring pair for interstereo, and opposite pair for cross-site). Inconsistencies between adjacent site frames appear to be systematic. Therefore we apply a transformation (translation and rotation without scale change) to the last site frame based on cross-site tie points to ensure that better initial pointing information of the BA network is achieved for convergence.

[29] Data for localization and BA have been collected consistently at the Gusev crater landing site. Postdrive Navcam 3 × 1 (3 columns by 1 row) mosaics in the driving direction and 3 × 1 mosaics in the rear-looking direction were collected for site characterization and rover navigation. Alternatively, postdrive 360° Navcam and Pancam panoramic mosaics were taken when desirable for other science exploration. During long drives, for example, over 60 m, a middle point survey (four Navcam images separated by 45°) or rear-looking Pancam observation (3 × 1) at the end was commanded. Bundle adjustment of the rover traverse was performed regularly. Figure 9 shows the Spirit rover traverse up to sol 440. The line with triangular points is the traverse generated from telemetry that includes the improvement through VO, while the line with circular points is the

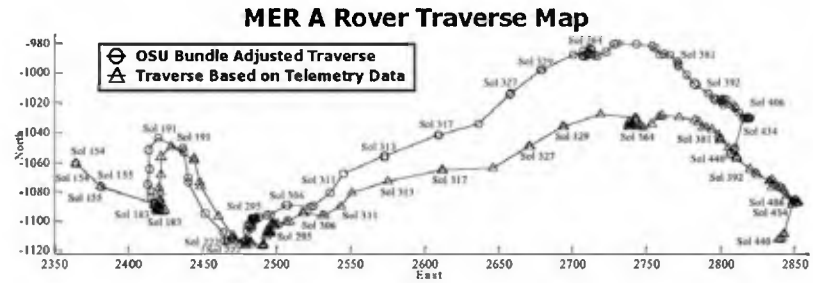

Figure 10. Spirit rover traverse in Husband Hill area from sol 154 to sol 440. Great slippages were experienced, and therefore the traverse error increased during this period. Bundle adjustment (BA) was able to correct relative errors as large as 10.5%.

Figure 11. Husband Hill traverse image map generated by projection of the bundle-adjusted rover positions onto the image mosaic.

bundle-adjusted traverse. The sol numbers are also shown on the map. The accumulated difference between these two traverses at the end is 56 m, or 1.5% of the traveled distance from the landing center, with a maximum of 2.7% (20.6 m over 775.7 m) on sol 106.

[30] To track the positions and errors during the climbing of Husband Hill, we performed a local comparison of rover traverses in the Husband Hill area starting from sol 154. Figure 10 shows the telemetry traverse (line with triangular points) and bundle-adjusted traverse (line with circular points) from sol 154 to sol 440. We can observe a significant error accumulation caused by wheel slippage. The locally accumulated difference between these two traverses at the end is 66 m, or 8.7% of the traveled distance of 764.6 m from sol 154, with a maximum of 10.5% (56.6 m over 540.6 m) on sol 337. We also produced traverse image maps by back projection of rover positions onto the image mosaics. Figure 11 shows the Spirit traverse of Husband Hill up to sol 373.

6. Topographic Mapping

[31] Topographic mapping of ground features and terrain along the traverse has been systematically performed. The BA results supply very high quality adjusted image pointing information (orientation parameters), which can be used to plot the 2-D rover traverse and the vertical profile of the traverse. Pancam and Navcam panoramas were used to produce ortho maps. As a byproduct of the ortho maps, digital terrain models were generated. Whenever ground features such as craters can be identified in MOC NA orbital images, the ortho maps along the traverse are compared with the orbital mosaic. The orbital map was corrected several times, for instance at about 200 m, 2.8 km, and 3.4 km along the traverse when the discrepancy between the BA traverse and orbital maps grew to be too large (over 10 m). On sols 85 and 223, two MOC NA images of the landing site were acquired. The rover track appeared as a faint dark linear feature across the mosaic of the two images. A preliminary comparison study of the bundle-adjusted traverse and that on the MOC NA image was carried out. The shape and the scale of the bundle-adjusted rover traverse and the track on the MOC mosaic match well, but there is a 1.3° relative rotation. We georeferenced the MOC mosaic to MDIM through THEMIS images. As a result, the maximum difference between the two traverses is about 90 m over an overall traverse of 3.11 km (2.89%). MDIM has an accuracy of ~230 m. There is error accumulation in the chain of rectification from THEMIS image to MDIM (1–2 THEMIS pixels, 18–36 m) and MOC image to THEMIS image (2–4 MOC pixels, 2–4 m). Considering the MOC image error and the accumulated georeferencing errors, the maximum difference of 90 m is within expectations.

6.1. Ortho Map Generation

[32] The average distance between two site frames at the Spirit site (up to sol 440) is about 35 m, with some individual distances of over 100 m. Using these panoramic

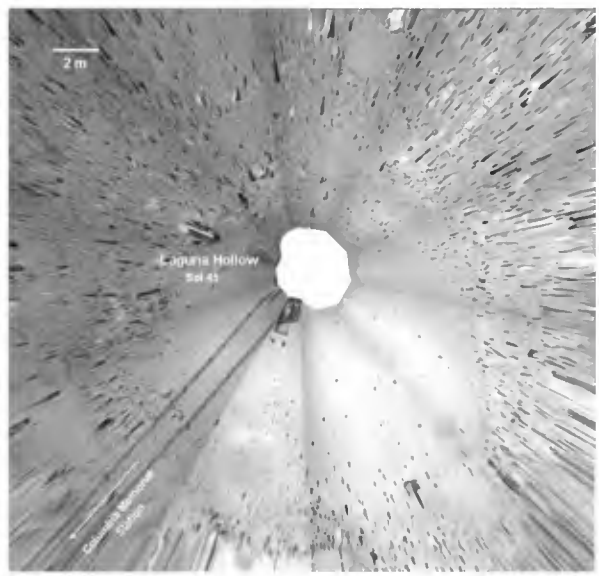

Figure 12. Ortho map of Laguna Hollow on sol 45 (60 m × 60 m, 1 cm/pixel). The ortho map has correct scale and orientation. Detailed information surrounding the rover, such as rocks and dunes, are in the right places and can be viewed in context (see also Figure 5b).

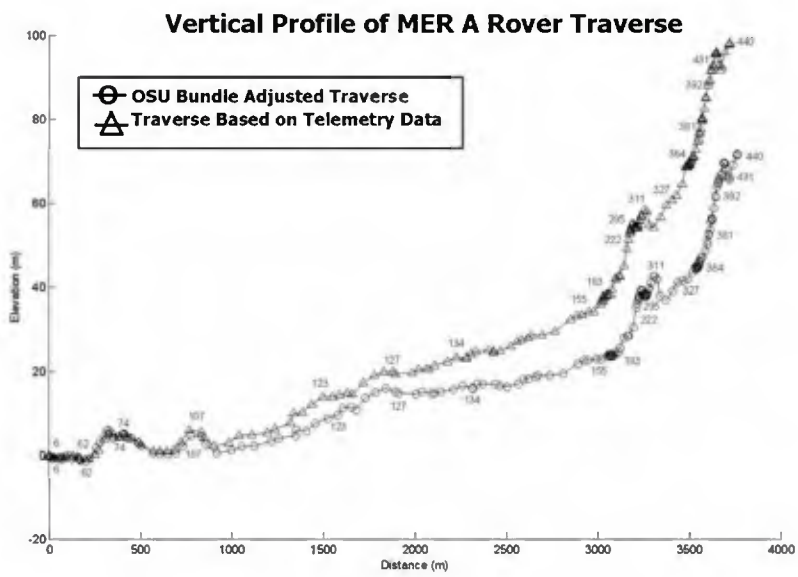

Figure 13. Vertical profile of the Spirit rover traverse (up to sol 440). The line with triangular points is computed from telemetry data, and the line with circular points is the resulted/corrected profile by the bundle adjustment method.

images, we generated ortho maps, each of which covers an area of 120 × 120 (Pancam) or 60 × 60 (Navcam) m. Detailed rock locations, orientation, and map scale are all correctly presented in the ortho map. Consecutive ortho maps connected along the traverse describe the large-scale topography across the landing site (Figure 5b).

[33] The generation of ortho maps consists of five steps: (1) registration of interest points between intrastereo images; (2) calculation of 3-D locations of the matched interest points; (3) construction of a triangular irregular network (TIN) using the 3-D matched points; (4) construction of a digital terrain model (DTM) (a grid) through an interpolation from the TIN; and (5) generation of the ortho map through projection between the images and the DTM.

[34] Contrast and intensity distribution of the panoramic images generally change due to different illumination conditions. A special method was developed to build balanced image sets for the ortho map by adjusting dynamic range and mean intensity over the interstereo tie points. If a bundle adjustment is performed, interstereo tie points suppress inconsistencies between adjacent stereo pairs and thus, a seamless (subpixel inconsistency) ortho map can be produced. Figure 12 shows an ortho map of Laguna Hollow on sol 45 with a resolution of 1 cm.

6.2. Vertical Profiles

[35] To illustrate the terrain relief along the rover traverse, a vertical profile was generated and expanded as the rover traversed. The horizontal position and elevation information was taken from the bundle adjustment results. Figure 13 shows the Spirit vertical profile up to sol 440. The horizontal axis of the figure is the distance traveled from the lander, and the vertical axis depicts elevation (scaled). Again, the line with tringular points is the profile computed from telemetry data and the line with circular points shows the BA result. The accumulated elevation difference is 26.4 m over a traveled distance of 3.76 km. This difference may be attributed to wheel slippage and IMU drift. The total elevation gain achieved by the rover over 440 sols, as shown by the BA result, is 72 m.

6.3. Mapping With Orbital Data

[36] MOC NA images were used to produce DTMs of representative terrains in candidate MER landing sites before the landing [*Kirk et al.*, 2003]. Although the high resolution of the MOC NA images (~3 m for the majority of images acquired with 2 × 2 pixel averaging) results in very high quality DTMs (10 m grid spacing), the small size of the images (maximum swath width 3 km) means that overlapping images suitable for stereo analysis (consisting of one nadir and one oblique image, or two suitable oblique images covering the same area) are rare. Only about 1100 useful pairs are currently known planet wide [*Kirk et al.*, 2004]. Even in the selected MER sites, which were targeted repeatedly by MOC, stereo coverage is not continuous but consists of isolated terrain samples. Neither MER spacecraft landed in an area for which stereo coverage existed beforehand.

[37] Useful MOC stereo coverage was, however, available for a region near the MER A landing point that is now being explored by the Spirit rover. A nadir image (E03-00012) showing the Columbia Hills with a coating of light-colored dust and an oblique image (E16-01962) of the same area in which the coating was partly removed by wind (dust devil) activity were identified prior to landing. The differences in surface appearance, as well as partial saturation of the second image, precluded the use of automatic stereo matching on this pair, but a useful DTM of part of the hills was obtained by manual editing. An unsaturated oblique image (R02-00357) was subsequently identified. In this image, more dust has been stripped away, resulting in a relatively uniform (but lower) albedo distribution that resembled the nadir view closely enough to permit a DTM to be generated by automatic matching with only

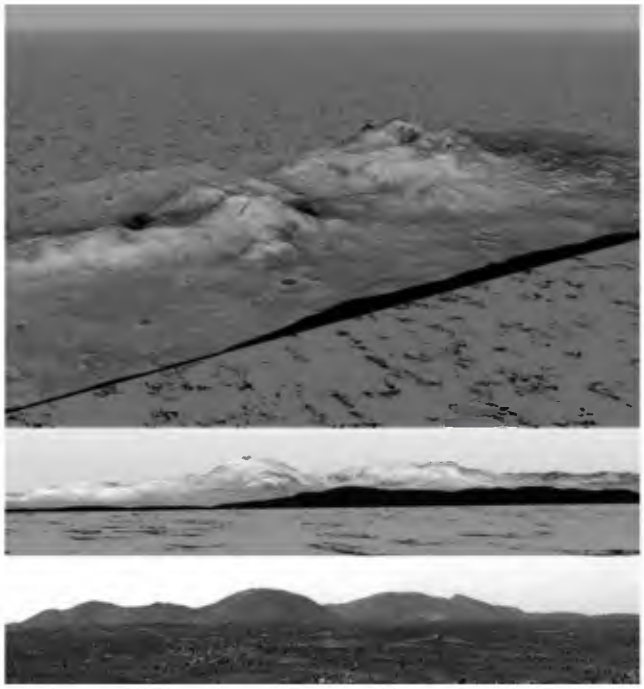

Figure 14. Comparison of synthetic perspective views of the Columbia Hills, 1.8 km southeast of the Spirit landing point, based on DTM derived from MOC NA orbital images (top, view from azimuth of landing point but from above; middle, view from true azimuth and elevation), with "ground truth" (bottom, Pancam image mosaic). MOC NA image used in synthetic views has a resolution of ~3 m/pixel; DTM has 10 m sample spacing and 2 m expected vertical precision. The resolution of Pancam images of hills is ~0.5 m. Vertical exaggeration is 2 in all cases. Synthetic views have been colored to approximate the appearance of the Martian surface, and an artificial texture has been used in areas of no data.

localized manual editing. As illustrated in Figure 14, the detail in the MOC image and DTM compares favorably with Pancam images of the Columbia Hills from the landing point 1.8 km away. This data set was used in several ways in planning the operations of the Spirit rover. First, perspective views like those in Figure 14 were helpful in clarifying geologic relationships in the hills and hence in identifying promising locations for the rover to sample the full geologic diversity of the area. Second, quantitative slope estimates derived from the DTM were compared with the rover performance in order to design a traverse that could reach the interest points safely. Finally, line-of-sight calculations were performed from a number of locations in and near the hills to the Sun, to other points on the ground (Figure 15), and to the orbiting MGS and Odyssey spacecrafts. The duration and obliqueness of solar illumination dictate the amount of power available to operate the rover and were factors in choosing favorable locations for the rover to pause for extended periods. The visibility of surrounding areas was also a factor in designing the rover traverse; it is obviously highly desirable to view each traverse destination from the ground as well as from orbit before approaching it, so an optimal path proceeds through points of high visibility. Finally, the visibility of the orbiters limits the times at which they can be used to relay rover data to Earth.

7. Applications

7.1. Ohio State University Web Geographic Information System

[38] The team at the Ohio State University Mapping and GIS Laboratory uses its "MarsMapper" software system to generate mapping products and to provide bundle-adjusted rover localization information for both rovers. The mapping products and traverse information are organized and disseminated through a Web-based Geographic Information System (Web GIS) developed for this mission. These products include up-to-date ortho maps, DTMs, crater models, traverse maps, contour maps, georeferenced DIMES images, rover traverse maps, and rover positions (coordinates) as well as other special products requested by scientists and engineers. During the mission operations, the Web GIS has tracked and corrected rover positions, and provided the information with appropriate MOC NA, DIMES, or ground ortho maps as a background (Figure 16). Newly collected images, including Navcam, Pancam, Hazcam, and MI images, are updated and georeferenced with the traverse and represented as image pointing lines, clicking on which results in display of the images within a georeferenced environment.

[39] The Web GIS was developed using both HTML and ArcIMS (©ESRI), an ESRI program that can deliver dynamic maps and GIS data and services via the Internet.

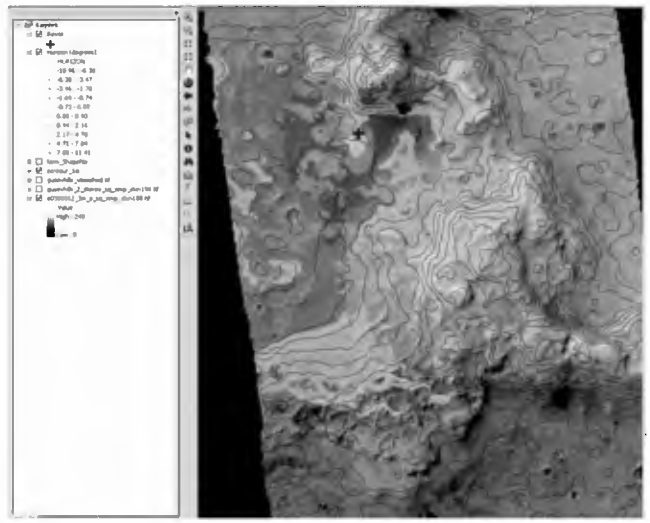

Figure 15. Example of line-of-sight calculation for part of Columbia Hills used for planning Spirit rover traverse. Base is orthorectified MOC image E03-00012, with 10 m elevation contours. The view shed for a hypothetical rover position on a spur south of the northern range of hills (yellow dot) is shown, with shading indicating the view angle above/below horizontal. High visibility of the surrounding terrain is desirable for obtaining rover images to plan further exploration; obscuration of the sky by features above the horizon can reduce both available solar power and communication opportunities with the MGS and Odyssey orbiters.

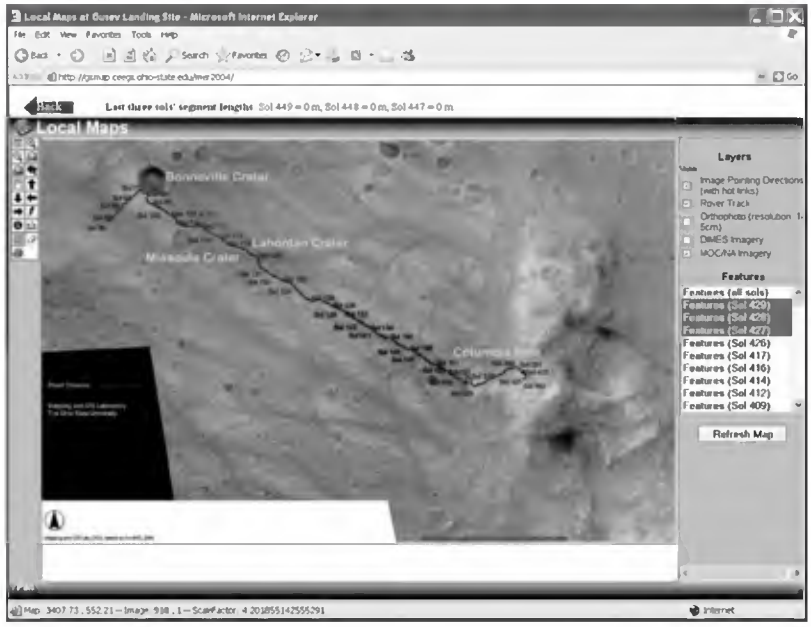

Figure 16. One of the interfaces of the Web GIS for accessing Spirit traverse information and local topographic products. Traversed segment distances of the last three sols are on the top. Tools for general GIS operations such as zoom, pan, map extend, simple query, distance measurement, and others are on the left. Layer legend and features, defined by scientists and organized in sols, are on the right. When zoomed to a detailed level, image pointing and sensor type information is represented by lines of different patterns at the rover positions.

Using ArcIMS, maps and features are ordered in different layers. Tools such as zoom, pan, hyperlink, identification, and measurement are employed to explore the mapping products. The Web GIS is password protected and accessible to the MER science and engineering teams. The system updates mapping products nearly every sol. Information about the rover locations for the three most recent sols is highlighted. The rover positions calculated from the telemetry data are updated each sol as well. The bundle-adjusted rover position requires a period (a few sols) which allows all necessary images (usually with lower downlink priority) to be downlinked from the spacecraft. In addition to the local mapping products, this web GIS provides access to global landing site information as well. Orbital imagery, such as MOC NA, THEMIS, and Viking images, MDIM maps and 3-D ChromaDepth maps of the landing site are presented as various layers of the GIS.

7.2. Strategic Planning and Data Analysis in Context

[40] Accurate localization conveys multiple benefits, both to planning activities on the tactical timescale (sol by sol) and also to the long-term objective to create a robust data set for the entire mission. Examples of each of these are summarized.

[41] The long drive by Spirit from the south rim of Bonneville crater to the foot of West Spur in the Columbia Hills was optimized by precise localization (Figures 5 and 16). The MER team concluded that exploration of Columbia Hills had the potential to enhance our understanding of the history of water at the Spirit landing site; thus the long traverse to the hills was warranted. However, in order to explore the vast Columbia Hills region, the traverse had to be achieved rapidly to conserve assets such as rover hardware and to work effectively with the ever-declining solar energy budget. Between sols 106 and 156, Spirit maintained a net bearing of about 120° and traversed the straight line distance of 2100 m from the northern rim of Missoula crater to the West Spur. The wheel odometry during this interval was not much more, only 2487 m. Spirit arrived at West Spur on sol 156, earlier than the planned target date of sol 160 (15 June 2004). Routine science

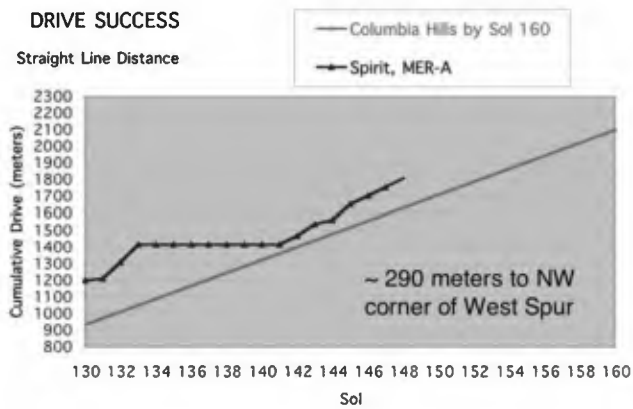

Figure 17. Plot of the cumulative drive progress (black line) of Spirit rover toward West Spur, Columbia Hills, and Gusev crater. The diagonal shaded line indicates the progress required to arrive at West Spur by sol 160, an objective that was established at the onset of the traverse. This particular chart indicates that on sol 148, Spirit was ahead of schedule. This metric allowed the science observations to be optimized during the traverse.

observations that were conducted during the traverse contributed to this timely arrival. Examples include the middle point survey Navcam images and rear-looking Pancam images, which were critical for the successful BA of the traverse. Precise localization allowed Spirit to achieve the maximum number of observations possible without compromising the driving schedule. During each sol's planning, Spirit's progress was reported in terms of the straight line distance remaining between the rover and the base of the West Spur (Figure 17). The Science Operations Working Group (SOWG) used this localization information to optimize the net azimuth of each drive and to design each installment of science observations in a way that was consistent with the scheduled date of arrival at the West Spur. The richness of these science observations reflects at least in part the key role that the localization campaign played in the tactical planning process. For example, because localization data indicated that Spirit was ahead of schedule, the SOWG elected to use the rover wheels to excavate a trench on sol 135. Spirit measured high concentrations of Mg and S in this trench [*Haskin et al.*, 2005], which had important implications for understanding the history of water and soluble salts in the regolith of Gusev crater.

[42] An optimal data set for a rover traverse should include accurate, systematic science observations that can be placed within the context of an accurate 3-D terrain model. The resolution of this terrain model must be sufficient to support the particular needs of any science observations. If a postmission analysis of an observation creates a new discovery, it should be possible to examine the terrain surrounding the site where the observation had been made in order to determine the geologic context for the discovery and maybe to achieve additional discoveries. The imaging that was made to support the localization campaign benefited the mission science data set in several ways. The imaging allowed a 3-D terrain model to be constructed that will provide geographic contexts for the science observations. The resolution of the Pancam and Navcam images is, in most cases, sufficient also to provide a detailed context for these observations at local, smaller scales. In summary, the localization campaign has insured that a database of images now exists to support research and discovery for years to come.

7.3. Geological Application

[43] An important goal of geologic analysis of rover data is development of "ground truth" for orbital remote sensing data sets. In practice this involves correlation of characteristics identified in orbital data with the characteristics as seen at the surface. Localization of the rover within orbital data sets is essential to this correlation.

[44] During the traverse across the plains from Bonneville crater to the Columbia Hills (Figure 16), several geologic features identifiable in MOC and THEMIS image data were crossed. These included impact craters and associated ejecta sheets, variations in apparent albedo and texture of the plain's surface, and differences in surface thermophysical properties. From the perspective of the rover, variations in clast morphology, distribution, and sizes; differences in soil abundance; and occurrences of small impact craters ("hollows") and excavated debris were identified in local Navcam and Pancam frames and panoramas [*Crumpler et al.*, 2005]. Once the location of each rover observation site was determined, it was mapped onto the MOC and THEMIS images and the corresponding observation compared with geologic maps prepared from the orbital remote sensing data.

[45] Several significant correlations identified include the surface manifestations of apparent radial differences in impact crater ejecta [*Grant et al.*, 2004; *Crumpler et al.*, 2005] and surface characteristics of variations in thermal characteristics. Geologic mapping of impact craters on Mars from orbital images in the past have shown that individual ejecta sheets may be divided into two components based on the morphology of the ejecta, an inner part between the crater rim and approximately two crater radii from the crater center that has been characterized as "continuous ejecta" and an outer part between approximately two crater radii and three crater radii characterized as "discontinuous ejecta." Traverse localization indicated that Spirit crossed these divisions on Bonneville crater, Missoula crater and Lahontan crater twice in each case. It was not known whether these divisions were sharp geologic contacts as they appeared from orbital data or gradational at some scale below the resolution of existing orbital data. On the basis of accurate localization of rover observation sites during the traverse, these divisions can be shown to occur across boundaries that are in fact only a few meters wide. In addition, the corresponding variations in clast size distribution across the ejecta sheets were possible since localization enabled a site-by-site mapping of observed distributions from rover observations with positions within the ejecta sheets.

[46] Variations in thermophysical properties in THEMIS data implied possible differences in the distribution of clasts and soils along the traverse. In general these data indicated that the ejecta of well-preserved craters in orbital data, which are by morphological definition young, are generally clast-rich, in other words "rockier." A notable exception was Lahontan crater, where THEMIS indicated relatively finer materials throughout the ejecta sheet. Location of the traverse observation sites within the THEMIS data set confirmed that the fines component was greater, yet the twofold division of the crater ejecta noted in Bonneville and Missoula also occurred. In addition, variations in thermophysical properties in THEMIS data of the intervening plains, particularly between Lahontan crater and the Columbia Hills, were of interest because there were few correlatable geological characteristics in orbital images over this part of the traverse and observations at the surface indicated relatively few distinctions between sites. Combining detailed locations of observation sites with position within the orbital data implied that subtle differences in small impact craters and local topography were likely responsible for influencing local fines accumulation.

[47] Furthermore, systematic surveys of wind-related features have been useful for characterizing transportation and organization of sand and dust on the floor of Gusev crater [*Greeley et al.*, 2004]. By providing a consistent frame of reference, localization has enabled an accurate assessment of the orientation of wind-related features that are separated by more than 3 km. Without this ability the observations would be treated as isolated sets rather than as part of a

systematically associated wind regime. Some aeolian features, such as dust devil tracks and crater wind streaks, are difficult to see from the surface but are visible in orbiter images. Reliable localization, coupled with the high-resolution MOC, THEMIS, and Mars Express images, enabled us to relate small- and large-scale features to time of formation and modification.

8. Conclusions

[48] This paper summarizes the achievements of localization and topographic mapping efforts of the MER mission (Spirit rover) up to sol 440. Successful localization of the lander within seven sols after landing and verification by MOC NA orbital images supported science planning in the early stage of surface operations. Visual odometry has been used frequently to give accurate rover locations when driving toward a target, and has demonstrated its ability to detect the significant slippage that the rover sometimes experiences. Incremental bundle adjustment built a global image network of each rover traverse to reduce the accumulated rover position errors and was used to correct position errors. The visual odometry and bundle adjustment results and orbital images ensured that the topographic mapping products of the landing site were generated with a high quality. The processed images, maps, DTMs and rover traverses have been utilized for strategic planning and tactical operations. The localization and topographic mapping results benefited a number of science application areas.

[49] **Acknowledgment.** This work is partially performed at the Jet Propulsion Laboratory, California Institute of Technology, under a contract with the National Aeronautics and Space Administration. The work has been supported by NASA through the Mars Exploration Program.

References

Arvidson, R. E., et al. (2004), Localization and physical properties experiments conducted by Spirit at Gusev crater, *Science*, *305*, 821–824, doi:10.1126/science.1099922.

Batson, R. M., and E. M. Eliason (1995), Digital maps of Mars, *Photogramm. Eng. Remote Sens.*, *61*, 1499–1507.

Bell, J. F., III, et al. (2006), In-flight calibration and performance of the Mars Exploration Rover Panoramic Camera (Pancam) instruments, *J. Geophys. Res.*, *111*, E02S03, doi:10.1029/2005JE002444.

Biesiadecki, J. J., and M. W. Maimone (2005), The Mars Exploration Rover surface mobility flight software: Driving ambition, in *Proceedings of the IEEE Aerospace Conference*, vol. 5, Inst. of Electr. and Electr. Eng., Big Sky, Mont.

Caplinger, M. A. (2005), Mars orbiter camera global mosaic, *Proc. Lunar Planet. Sci. Conf. 33rd*, abstract 1405.

Crumpler, L. S., et al. (2005), Mars Exploration Rover geologic traverse by the Spirit rover in the plains of Gusev crater, Mars, *Geology*, *33*(10), 809–812, doi:10.1130/G21673.1.

Di, K., and R. Li (2004), CAHVOR camera model and its photogrammetric conversion for planetary applications, *J. Geophys. Res.*, *109*, E04004, doi:10.1029/2003JE002199.

Di, K., F. Xu, R. Li, L. Matthies, and C. Olson (2002), High precision landing site mapping and rover localization by integrated bundle adjustment of MPF surface images, *Int. Arch. Photogramm. Remote Sens. Spatial Inf. Sci.*, *34*, 733–737.

Gennery, D. B. (1992), Least-squares camera calibration including lens distortion and automatic editing of calibration points, paper presented at the Workshop on Calibration and Orientation of Cameras in Computer Vision, XVII Congr. of the Int. Soc. of Photogramm. and Remote Sens., Washington, D. C., 2 Aug.

Golombek, M., and T. Parker (2004), Lander localization, MER project memorandum, Jet Propul. Lab./NASA, Pasadena, Calif.

Grant, J. A., et al. (2004), Surficial deposits at Gusev crater along Spirit rover traverses, *Science*, *305*, 807–810.

Greeley, R., et al. (2004), Wind-related processes detected by the Spirit rover at Gusev crater, *Science*, *305*, 810–813.

Guinn, J. R., and T. A. Ely (2004), Preliminary results of Mars Exploration Rover in situ radio navigation, paper AAS 04-270 presented at the 14th Space Flight Mechanics Meeting, AAS/AIAA, Maui, Hawaii, 8–12 Feb.

Haskin, L. A., et al. (2005), Water alteration of rocks and soils from the Spirit rover site, Gusev crater, Mars, *Nature*, *436*(7047), 66–69.

Kirk, R. L., et al. (1999), Mars DIM: The next generation, *Proc. Lunar Planet. Sci. Conf. 30th*, abstract 1849.

Kirk, R. L., E. M. Lee, R. M. Sucharski, J. Richie, A. Grecu, and S. K. Castro (2000), MDIM 2.0: A revised global digital image mosaic of Mars, *Proc. Lunar Planet. Sci. Conf. 31st*, abstract 2011.

Kirk, R. L., E. Howington-Kraus, B. Redding, D. Galuszka, T. M. Hare, B. A. Archinal, L. A. Soderblom, and J. M. Barrett (2003), High-resolution topomapping of candidate MER landing sites with Mars Orbiter Camera narrow-angle images, *J. Geophys. Res.*, *108*(E12), 8088, doi:10.1029/2003JE002131.

Kirk, R. L., E. Howington-Kraus, T. Hare, R. Soricone, K. Ross, L. Weller, M. Rosiek, B. Redding, D. Galuszka, and B. A. Archinal (2004), High-resolution topomapping of Mars: Life after MER site selection, *Proc. Lunar Planet. Sci. Conf. 35th*, abstract 2046.

Li, R., F. Ma, F. Xu, L. H. Matthies, C. F. Olson, and R. E. Arvidson (2002), Localization of Mars rovers using descent and surface-based image data, *J. Geophys. Res.*, *107*(E11), 8004, doi:10.1029/2000JE001443.

Li, R., K. Di, and F. Xu (2003), Automatic Mars landing site mapping using surface-based images, paper presented at the ISPRS WG IV/9: Extraterrestrial Mapping Workshop on Advances in Planetary Mapping, Houston, Tex., 22 March.

Li, R., K. Di, L. H. Matthies, R. E. Arvidson, W. M. Folkner, and B. A. Archinal (2004), Rover localization and landing site mapping technology for 2003 Mars Exploration Rover mission, *Photogramm. Eng. Remote Sens.*, *70*, 77–90.

Ma, C., E. F. Arias, T. M. Eubanks, A. L. Fey, A.-M. Gontier, C. S. Jacobs, O. J. Sovers, B. A. Archinal, and P. Charlot (1998), The international celestial reference frame as realized by very long baseline interferometry, *Astron. J.*, *116*, 516–546.

Neumann, G. A., D. D. Rowlands, F. G. Lemoine, D. E. Smith, and M. T. Zuber (2001), The crossover analysis of MOLA altimetric data, *J. Geophys. Res.*, *106*, 23,723–23,735.

Olson, C. F., L. H. Matthies, M. Schoppers, and M. W. Maimone (2003), Rover navigation using stereo ego-motion, *Robotics Auton. Syst.*, *43*, 215–229.

Parker, T., et al. (2004), Localization, localization, localization, *Proc. Lunar Planet. Sci. Conf. 35th*, abstract 2189.

Seidelmann, P. K., et al. (2002), Report of the IAU/IAG working group on cartographic coordinates and rotational elements of the planets and satellites: 2000, *Celestial Mech. Dyn. Astron.*, *82*, 83–110.

U.S. Geological Survey (1991), Mission to Mars: Digital image maps [CD-ROM], *PDS Vol. VO 2001–VO 2007*, Washington, D. C.

Xu, F., K. Di, R. Li, L. Matthies, and C. Olson (2002), Automatic feature registration and DEM generation for Martian surface mapping, *Int. Arch. Photogramm. Remote Sens. Spatial Inf. Sci.*, *34*, 549–554.

Yakimovsky, Y., and R. Cunningham (1978), A system for extracting three-dimensional measurements from a stereo pair of TV cameras, *Comput. Graphics Image Process.*, *7*, 195–210.

B. A. Archinal, R. L. Kirk, and L. A. Soderblom, U.S. Geological Survey, Flagstaff, AZ 86001, USA.

R. E. Arvidson, Department of Earth and Planetary Sciences, Washington University, St. Louis, MO 63130, USA.

J. Bell and S. W. Squyres, Department of Astronomy, Cornell University, Ithaca, NY 14853, USA.

P. Christensen, R. Greeley, and S. Thompson, Department of Geological Sciences, Arizona State University, Tempe, AZ 85287, USA.

L. Crumpler, New Mexico Museum of Natural History and Science, Albuquerque, NM 87104, USA.

D. J. Des Marais and M. Sims, NASA Ames Research Center, Moffett Field, CA 94035, USA.

K. Di and R. Li, Department of Civil and Environmental Engineering and Geodetic Science, Ohio State University, Columbus, OH 43210, USA. (li.282@osu.edu)

T. Duxbury, M. Golombek, J. Guinn, A. Johnson, M. Maimone, L. H. Matthies, and T. Parker, Jet Propulsion Laboratory, Pasadena, CA 91109, USA.

J. Grant, Smithsonian Institution, Washington, DC 20560, USA.

M. Malin, Malin Space Science Systems, San Diego, CA 92191, USA.